Achieving atomically ordered GaN/AlN quantum heterostructures: The role of surface polarity

Article *in* Proceedings of the National Academy of Sciences · October 2023

DOI: 10.1073/pnas.2303473120

7 authors, including:

Yuanpeng Wu
University of Michigan
58 PUBLICATIONS **1,197** CITATIONS
SEE PROFILE

Ding Wang
University of Michigan
63 PUBLICATIONS **770** CITATIONS
SEE PROFILE

Ping Wang
139 PUBLICATIONS **1,864** CITATIONS
SEE PROFILE

PNAS RESEARCH ARTICLE | ENGINEERING

Achieving atomically ordered GaN/AlN quantum heterostructures: The role of surface polarity

Yuanpeng Wu[a,1], Peng Zhou[a,1], Yixin Xiao[a,1], Kai Sun[b], Ding Wang[a], Ping Wang[a], and Zetian Mi[a,2]

Edited by Zhenqiang Ma, University of Wisconsin-Madison, Madison, WI; received March 1, 2023; accepted September 19, 2023 by Editorial Board Member John A. Rogers

Interface engineering in heterostructures at the atomic scale has been a central research focus of nanoscale and quantum material science. Despite its paramount importance, the achievement of atomically ordered heterointerfaces has been severely limited by the strong diffusive feature of interfacial atoms in heterostructures. In this work, we first report a strong dependence of interfacial diffusion on the surface polarity. Near-perfect quantum interfaces can be readily synthesized on the semipolar plane instead of the conventional *c*-plane of GaN/AlN heterostructures. The chemical bonding configurations on the semipolar plane can significantly suppress the cation substitution process as evidenced by first-principles calculations, which leads to an atomically sharp interface. Moreover, the surface polarity of GaN/AlN can be readily controlled by varying the strain relaxation process in core–shell nanostructures. The obtained extremely confined, interdiffusion-free ultrathin GaN quantum wells exhibit a high internal quantum efficiency of ~75%. Deep ultraviolet light-emitting diodes are fabricated utilizing a scalable and robust method and the electroluminescence emission is nearly free of the quantum-confined Stark effect, which is significant for ultrastable device operation. The presented work shows a vital path for achieving atomically ordered quantum heterostructures for III-nitrides as well as other polar materials such as III-arsenides, perovskites, etc.

heterointerface | surface polarity | atomic substitution | quantum efficiency | quantum-confined Stark effect

Significance

A strong dependence of interfacial diffusion on surface polarity is observed in GaN/AlN quantum heterostructures. GaN/AlN quantum heterostructures with near-perfect quantum interface are achieved on the semipolar plane. Theoretical calculations show that the atomic substitution process is significantly suppressed on the semipolar plane compared with the conventional *c* -plane. Interdiffusion-free ultrathin GaN exhibits efficient luminescence and is nearly free of the quantum-confined Stark effect. The controlled incorporation sites can be achieved through varying surface polarities in nanostructures.

Semiconductor heterostructures, stacked by two or more dissimilar materials, have been extensively explored in controlling band structure (1, 2), polarization field (3, 4), strain distribution (5, 6), charge carrier confinement and mobility (7, 8), and excitonic oscillator strength (9, 10), which can provide material properties that are superior or not possible otherwise (11–13). A significant challenge in unlocking the potential of atomic-scale heterostructures is the presence of atomic substitution processes among cations with different ionicity at the heterointerface (14), which leads to interfacial composition gradients or formation of nanoclusters, preventing the realization of atomically ordered quantum heterostructures (15–17). A diffusive interface causes a reduction in electron mobility due to alloy scattering in high electron mobility transistors (18, 19) and significantly broadened emissions and slow radiative recombination in light-emitting diodes (17, 20). Extensive theoretical analysis and experimental synthesis have been devoted to improving the interface quality (21–27). Despite the improvements in synthesis methods and parameters, the presence of diffusive layers remains widely observed (22–24, 28, 29), which have been attributed to surface segregation (22, 26), composition pulling effect (24), and high synthesis temperature (30).

In this work, we show, both experimentally and theoretically, that interfacial diffusion in GaN/AlN heterostructures strongly depends on the surface polarities. Ultrathin GaN/AlN digital alloys with nearly diffusion-free heterointerfaces can be synthesized on the semipolar plane, in contrast to the severe interfacial diffusion observed on the conventional *c*-plane. Atomically ordered quantum heterostructure features superior optical properties including high internal quantum efficiency and absence of quantum-confined Stark effect. Moreover, the surface polarities can be readily controlled by varying the strain relaxation process in the core–shell nanostructure ensembles.

Results

Epitaxy and Structural Characterizations. The study is performed on a nanostructure platform and under nitrogen-rich conditions wherein the strain effect is mitigated (31, 32). Ultrathin GaN/AlN quantum wells (QWs) in AlN nanowire ensembles on Si substrate were grown by plasma-assisted molecular beam epitaxy (PAMBE). The epitaxy includes an initial spontaneous formation of a GaN nanowire template for promoting the nanowire

Competing interest statement: The University of Michigan and Mi have an ownership of equity in NS Nanotech and NX Fuels, which have licensed some IP related to this work, were co-founded by Mi, and have ongoing sponsored research projects in Mi's lab at the University of Michigan. We filed a invention report titled "Surface Polarity-Controlled Atomically Ordered GaN/AlN Quantum Interface" on May 23, 2023. The University filed a provisional patent. Mi previously served as a member of Board of Directors of NS Nanotech.

This article is a PNAS Direct Submission. Z.M. is a guest editor invited by the Editorial Board.

[1]Y.W., P.Z. and Y.X. contributed equally to this work.

[2]To whom correspondence may be addressed. Email: ztmi@umich.edu.

This article contains supporting information online at https://www.pnas.org/lookup/suppl/doi:10.1073/pnas.2303473120/-/DCSupplemental.

Published October 24, 2023.

Table 1. Growth conditions of samples discussed in this work

Sample	GaN template duration (mins)	QW incorporation sites	Number of QWs	GaN QW thickness (MLs)	AlN barrier thickness (MLs)
A1	60	*c*-plane	1	1	>40
A2	60	*c*-plane	5	2	6
B1	20	semipolar plane	10	2	18
B2	20	semipolar plane	5	2	6

morphology followed by an AlN segment before the growth of GaN/AlN QWs (33, 34). The samples studied in this work consist of two series that differ in the crystalline planes on which the GaN QWs are incorporated, i.e., Series A (B) samples have QWs on the *c*- (semipolar) plane. Growth details of the samples discussed in the main text can be found in Table 1 and *Materials and Methods*.

Fig. 1*A* shows the low-magnification high-angle angular dark field (HAADF) scanning transmission electron microscopy (STEM) image of sample A1 with a (monolayer) ML GaN QW embedded in an AlN nanowire. The ultrathin GaN QW is observed to be embedded on the flat *c*-plane of the AlN and intersects the entire nanowire. The high-resolution STEM image of the QW region (orange-boxed region) is shown in Fig. 1*B*, wherein the ML GaN forms an atomically sharp interface with the underlying AlN. However, random contrast variations are observed at the AlN-on-GaN interface, suggesting a strong intermixing of Al and Ga cations. Fig. 1*C* is the averaged line profiles across the interface (dash-boxed region in Fig. 1*B*), wherein random intensity variations up to 6 MLs are observed after ML GaN, as indicated by the shaded yellow region. The asymmetric interfacial abruptness has been widely observed in Al(Ga)N heterostructures synthesized using MBE (21–23) and metalorganic chemical vapor deposition (MOCVD) (13, 24). Although the QW remains distinct when separated by thick AlN barriers, the intermixing issue is exacerbated when the thickness of the AlN barrier is comparable to, or smaller than the cation diffusion

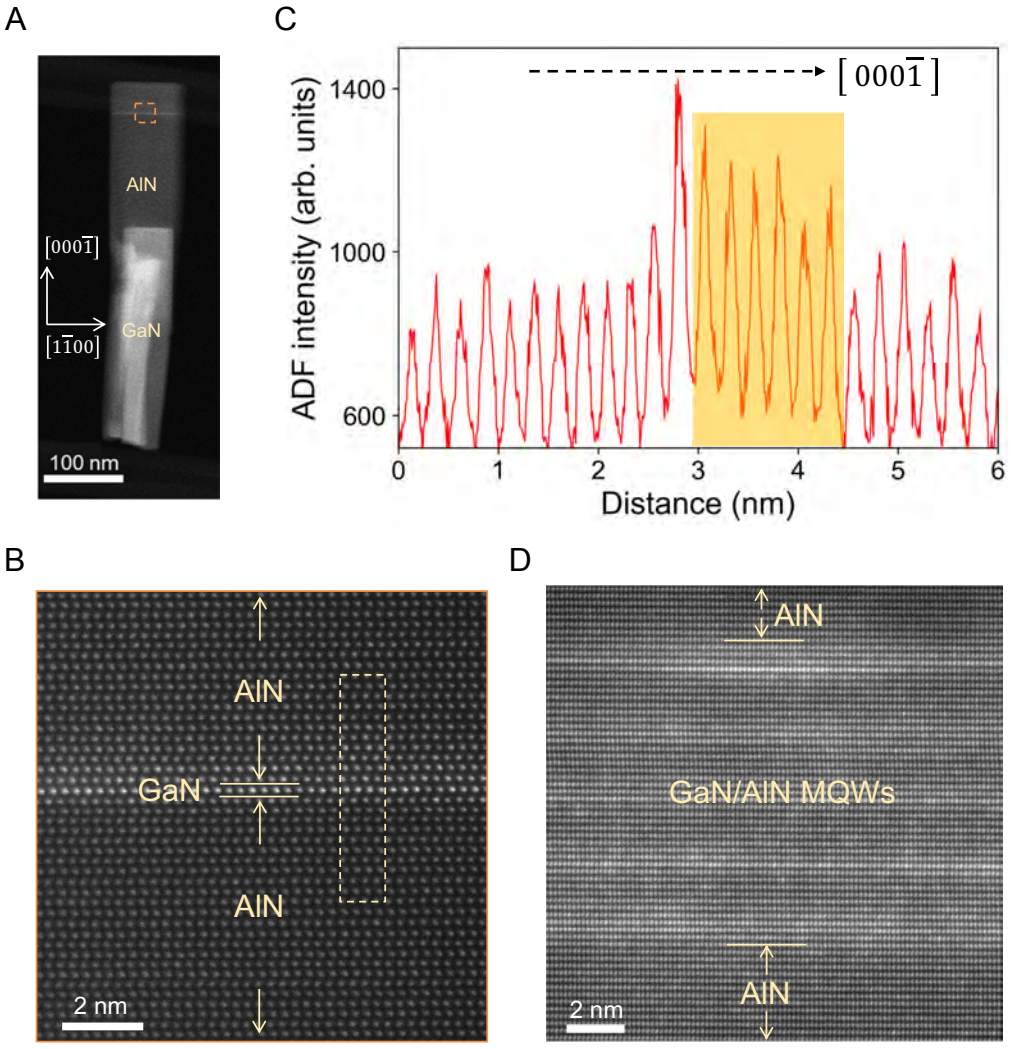

Fig. 1. Structural characterization of GaN/AlN quantum heterostructures on *c*-plane. (*A*) Low-magnification HAADF-STEM image of monolayer GaN incorporated on the *c*-plane of an AlN nanowire. (*B*) High-resolution HAADF-STEM image of the orange-boxed region in (*A*). The ML GaN as well as the AlN barriers are indicated by the arrows. (*C*) ADF intensity analysis of the yellow-boxed region in (*B*). The yellow-shaded region indicates the cation intermixing region. (*D*) HAADF-STEM image of five periods of digital alloys of 2 MLs GaN/6 MLs AlN (sample A2).

length. Sample A2 has a designed active region of five periods of 2 MLs GaN/6 MLs AlN. However, the GaN QWs can be barely distinguished in the high-resolution STEM image as shown in Fig. 1*D*. It is worth mentioning that the interdiffusion even occurs at a much lower growth temperature as shown in *SI Appendix*, Fig. S1, indicating a low thermal activation energy of the atomic substitution process on the *c*-plane (35).

Next, we show that this issue can be alleviated by incorporating GaN QWs on semipolar planes. Fig. 2*A* shows the low-magnification HAADF-STEM images of sample B1, wherein the active region of the nanowire heterostructure consists of 10 periods of 2 MLs GaN/18 MLs AlN. Unlike the GaN/AlN digital alloys in Series A, the QWs are seen to be incorporated on $(1\bar{1}0\bar{3})$ semipolar planes while the growth is along the $[000\bar{1}]$ direction as shown in Fig. 2 *B*–*D*. In contrast to the smeared interface in Series A, Fig. 2*E* shows interfacial diffusion neither before nor after the GaN QW, which is further evidenced by the distinct contrast variation across the interface in the yellow-boxed region of Fig. 2*C*. This observation remains true for closely separated GaN QWs as shown in Fig. 2*F*, wherein the active region of sample B2 consisting of 2 MLs GaN/6 MLs AlN barriers is imaged by HAADF-STEM.

First-principles Density Functional Theory Analysis. The pronounced dependence of GaN/AlN interface quality on the incorporation plane is analyzed by investigating the chemical bonding configurations and atomic arrangements of the growth front. We consider that the two front facets of GaN, namely, $(000\bar{1})$ plane and $(1\bar{1}0\bar{3})$ plane in correspondence with the experiment, are covered by a 1 × 1 Al adlayer, as shown in Fig. 3 *A* and *B*. The structural models are based on previous studies for $(000\bar{1})$ (26, 36) and semipolar GaN surfaces (37). The obtained results show that the exchange of an Al adatom with a Ga atom from the first subsurface cation layer on the $(000\bar{1})$ plane, as indicated by the arrow and dashed red circles in Fig. 3*C*, provides an energy change of -2.74 eV, driving the cation substitution process over an extended distance, i.e., a diffusive interface. The Al adatoms on $(1\bar{1}0\bar{3})$ plane has two distinct types of sites in the surface layer. We refer to these sites as Al_{1C} and Al_{2C} sites as shown in Fig. 3*B*. The adatoms at the Al_{1C} sites are bonded to a single N atom in the layer below, which resembles the bonding configuration of Al adatom on the $(000\bar{1})$ surface. The Al adatoms at the Al_{2C} sites bond with two adjacent N atoms, one in the underlying $(000\bar{1})$ plane and another in the layer above. The Al adatoms in the two sites can substitute three-coordinated and four-coordinated Ga atoms (labeled as Ga_{3C} and Ga_{4C} in Fig. 3*B*). These four possible combinations of exchanges are schematically illustrated in Fig. 3 *D*–*G*, along with the corresponding calculated energy changes. The atomic exchange with the smallest energy reduction, $Al_{2C} \leftrightarrow Ga_{3C}$, is –1.04 eV, which is 1.7 eV less negative than that on the *c*-plane. Therefore, although the GaN/AlN digital alloys in samples B2 and A2 were grown using the same conditions, the less negative energy change in sample B2 can stabilize the Al adatoms on the semipolar plane and eliminate the diffusion at the interface. Moreover, the substitution process of Al and Ga in the deeper subsurface was also investigated (*SI Appendix*, Fig. S2). The result reveals that all energy changes

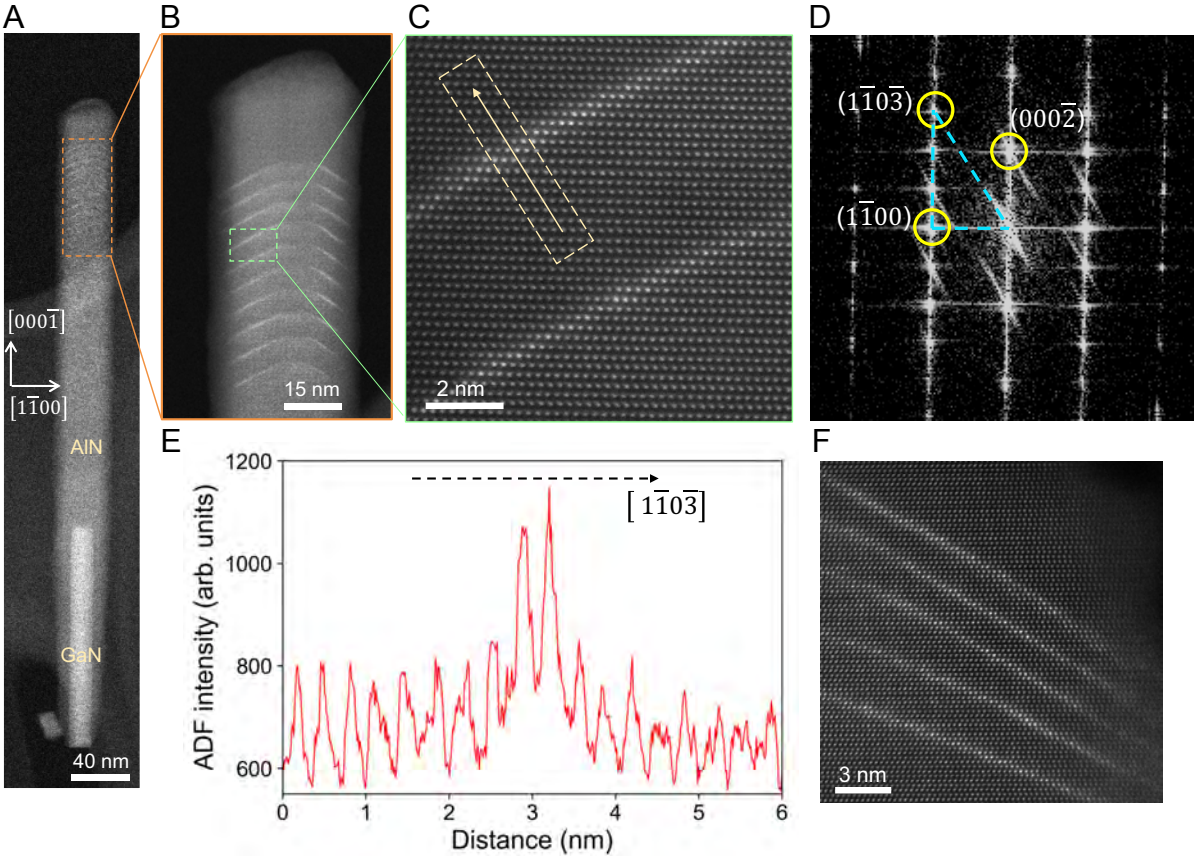

Fig. 2. Structural characterization of GaN/AlN quantum heterostructures on the semipolar plane. (*A*) Low-magnification HAADF-STEM image of 10 periods of GaN/AlN digital alloys embedded in an AlN nanowire. (*B*) HAADF-STEM image of the orange-boxed region in (*A*). (*C*) High-resolution HAADF-STEM image of the green-boxed region in (*B*). (*D*) Fast Fourier transform of (*C*). (*E*) ADF intensity analysis of the yellow-boxed region in (*C*). (*F*) HAADF-STEM image of the active region of sample B2 consisting of 2 MLs GaN/6 MLs AlN.

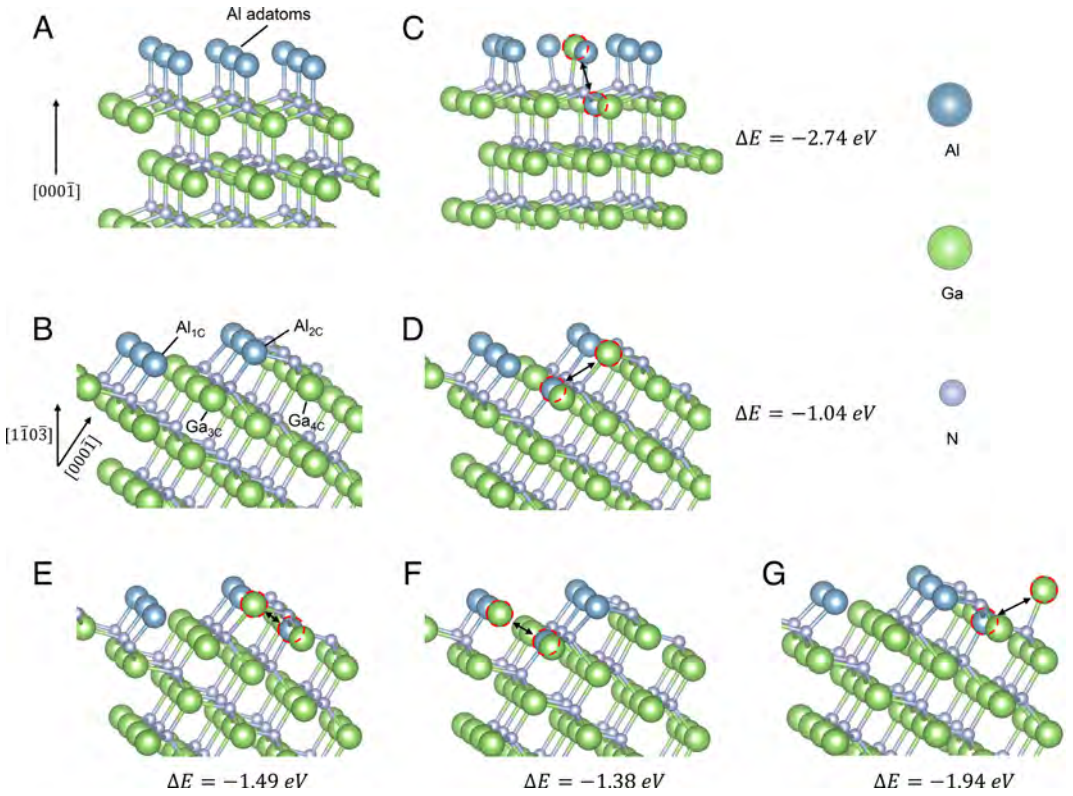

Fig. 3. First-principles density functional theory calculations of atomic arrangements on *c*-/semipolar planes. (*A*) Schematic of GaN (000$\bar{1}$) surface covered with Al adlayer. Each Al adatom forms one broken bond with the underlying N anion. (*B*) Schematic of Al adatoms on the (1$\bar{1}$0$\bar{3}$) surface of GaN, wherein the two-coordinated Al adatom labeled as Al_{2C} form two bonds with adjacent N anions while the one-coordinated Al adatom labeled as Al_{1C} forms one bond with adjacent N anion. The three (four)-coordinated Ga cation is labeled as Ga_{3C}(or Ga_{4C}), which forms three (or four) bonds with adjacent N anions. (*C*–*G*) Schematics of the cation exchanges along with the corresponding calculated energy changes. The dashed red circles enclose the Al adatom and the Ga cation involved in the substitution process.

in those models are close to zero, which can be attributed to the highly or fully coordinated Al or Ga in subsurface layers. Hence, the intrinsic coordination structures of the outmost surface layers instead of subsurface layers play the most significant role during heteroepitaxy.

Luminescence Properties and Analysis. With the attainability of GaN/AlN quantum heterostructure with a near-perfect interface on the semipolar plane, enhanced quantum confinement of charge carriers within the GaN QW is expected (38–40). Temperature-dependent photoluminescence (PL) measurements were performed on samples B2 and A2 under the same excitation conditions of 420 mW/cm^2 and the corresponding spectra are shown in Fig. 4*A* and *SI Appendix*, Fig. S3*A*. The origin of the emission peaks can be discerned through comparison with the spectra of AlN nanowires without embedded GaN QWs (*SI Appendix*, Fig. S3*B*), wherein the emission around 5.93 eV is related to the excitonic emission from AlN (41) and the emissions between 4.0 and 5.5 eV are related to the GaN/AlN digital alloys. The measured room-temperature peak energy of sample B2 is around 5.1 eV, larger than the peak energy of ~4 eV obtained from sample A2. The room-temperature internal quantum efficiency (IQE) is estimated by taking the integrated intensity ratio between room temperature and 12 K under the assumption that the IQE is unity at the lowest temperature (42, 43). The measured IQE of GaN/AlN digital alloys in sample B2 is ~75%, which is more than three times higher than the 23% IQE measured from sample A2. While the intended thickness of GaN/AlN digital alloys in both cases is the same, the Al–Ga intermixing on the *c*-plane (sample A2) leads to the formation of a wide Al(Ga)N QW with large inhomogeneity along with an increased probability to encounter nonradiative recombination centers and therefore a less efficient radiative recombination process (44, 45).

Considering GaN QW with a nominal thickness of 2 MLs and AlN barrier with a thickness of 6 MLs, the calculated internal electrostatic field can be up to ~10 MV/cm for GaN/AlN quantum wells. (Detailed calculations can be found in *SI Appendix*, section 4.) Despite this large built-in electric field, the QCSE is expected to be significantly suppressed in an atomically thin QW. The large band structure offset between GaN and AlN can provide extreme quantum-confinement of charge carriers and ensure excellent electron–hole wavefunction overlap under various carrier densities (33, 45). Indeed, the PL energy of sample B2 shows negligible shift with excitation power as shown by the blue squares in Fig. 4*B* and the spectra in *SI Appendix*, Fig. S3*C*. Meanwhile, a monotonic blue shift of the peak energy from 4.014 eV to 4.117 eV with excitation power was observed from sample A2 (green circles in Fig. 4*B* and the spectra in *SI Appendix*, Fig. S3*D*) as a result of the increasing screening of the QCSE (46, 47). Moreover, the complex spatial landscape for the electronic states could be formed during Al–Ga intermixing, which leads to the presence of localized states. With increasing excitation power, extra generated charge carriers tend to occupy the higher localized states, which also contribute to the blueshift in emission energies (48).

Deep UV (DUV) LED structures with 2 MLs GaN/6 MLs AlN on *c*-/semipolar plane as an active region were grown and fabricated as schematically shown in Fig. 4*C*. The fabrication involves a SiO_2 filling followed by a reactive etching process to define the current injection window, which is much more scalable and robust than the

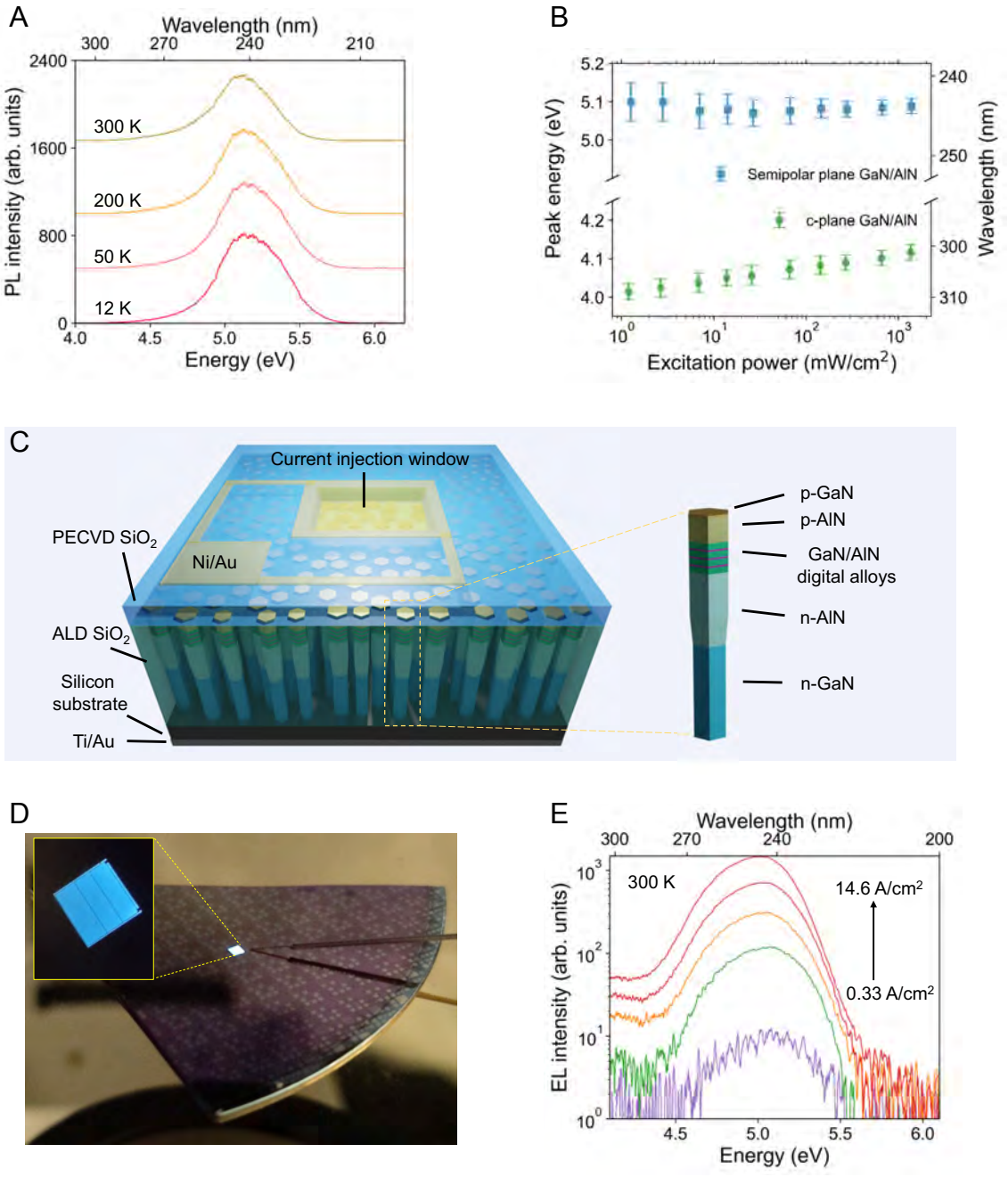

Fig. 4. Luminescence properties of GaN/AlN quantum heterostructures on the *c*-/semipolar plane. (*A*) Temperature-dependent photoluminescence (PL) spectra of sample B2 were measured with an excitation power of 420 mW/cm^2. (*B*) PL peak energy vs. excitation power for sample A2 (green circles) and B2 (blue squares). (*C*) Device schematic of deep UV LED-based on GaN/AlN heterostructures. (*D*) Optical images of a deep UV LED on a Si(111) substrate. (*E*) Current-dependent electroluminescence spectra of deep UV LED with semipolar plane GaN/AlN digital alloys as the active region.

previously reported tilted metal deposition method (33). Detailed sample information and fabrication process can be found in *Materials and Methods*. The current–voltage characteristics of devices based on *c*-/semipolar plane GaN/AlN show similar electrical properties including a rectification ratio of over 5 orders of magnitude at ±10 V as shown in *SI Appendix*, Fig. S4*A*. The typical current-dependent electroluminescence (EL) spectra of devices with semipolar GaN/AlN as an active region are shown in Fig. 4*D*. The peak energies show a slight red shift from 5.07 eV to 5.02 eV with increasing currents, which can be explained by heating effect-induced bandgap renormalization (3, 41). In contrast, DUV LEDs with *c*-plane GaN/AlN as active region show a significant blueshift with increasing injection current (*SI Appendix*, Fig. S4*B*) due to the reasons elaborated above.

Control of Surface Polarity of GaN/AlN Heterostructures. Finally, we discuss the crystalline origin of controlled surface polarity/incorporation sites of GaN/AlN heterostructures, i.e., *c*-plane versus semipolar plane. Among the samples characterized, it was observed that the orientation of embedded GaN QWs is parallel to the faceted top of the nanowire ensemble, as most clearly seen in Figs. 1 *A* and *2A*, suggesting the incorporation sites of GaN QWs are defined by the morphology of growth front of AlN segment. While the bottom GaN nanowire ensembles always have the flat $(000\bar{1})$ facet, the top facet of the AlN segment on GaN nanowire can be tuned between $(1\bar{1}0\bar{l})$ and $(000\bar{1})$ by varying the bottom GaN nanowire density. Experimentally, it was observed that the heteroepitaxy of AlN on GaN nanowires with a density

of ~4 × 10^{10} cm^{-2} can result in a flat facet, while a density of ~2 × 10^{10} cm^{-2} can lead to a convex semipolar facet. The growth front of various facets is generally attributed to the anisotropy of the growth rate along different crystalline axes and has been widely studied using Wuff's plot (49, 50). However, high-resolution annular bright field (ABF) characterizations on both samples from Series A and B show that the nanowires have the same growth direction of [000$\bar{1}$] orientation as shown in *SI Appendix*, Fig. S5, consistent with previous reports of III-nitride nanowires grown on Si substrate by MBE (51, 52).

Here, the varying top facet of AlN can be attributed to the different strain relaxation processes during the initial heteroepitaxy of the AlN nanowire on top of the GaN nanowire. AlN tends to be formed on both the top (*c*-plane) and sidewall (*m*-planes) of GaN nanowires due to the limited migration length of Al adatoms (53, 54). The coverage of the Al adatoms on the sidewall is greatly affected by the shadowing effect of adjacent nanowires. For GaN nanowire ensembles with high density (small spacing between neighboring nanowires), a thin and short AlN shell tends to be formed as schematically shown in *SI Appendix*, Fig. S6*A*. In this case, coherent biaxial tensile strain is stored in the AlN segment initially, and strain relaxation is achieved through the sidewalls as the AlN segment growth proceeds. For thick and long AlN shells formed as a result of low GaN nanowire ensemble density (larger nanowire spacing) (*SI Appendix*, Fig. S6*B*), the AlN shell at the sidewall causes a significant accumulation of strain, particularly at the periphery of the AlN segment, which leads to strain relaxation through generating high index facets (55). More detailed discussions can be found in *SI Appendix*.

Discussion

In conclusion, this study provides a vital strategy to achieve atomically ordered GaN/AlN quantum heterostructures by incorporating GaN on the semipolar plane of the AlN nanostructure. The first-principles DFT calculations show that the energy change after atomic exchanges on the semipolar plane is less negative than that on the *c*-plane, which effectively prevents interdiffusion between cations with different ionicity. The near-perfect interface between GaN and AlN ensures extreme quantum confinement and superior optical properties, including an IQE of 75% and negligible QCSE in both optically and electrically pumped devices. The origin of the varying incorporation planes is also studied and attributed to the different strain relaxation mechanisms in nanostructured GaN/AlN. The presented methods shed light on synthesizing high-quality digital alloy/superlattice not only for III-nitride materials but also other material systems such as III-arsenides, ABO_3 perovskites, and group IV heterostructures.

Materials and Methods

Epitaxy. Three-inch Si wafers with <111> orientations were used for the epitaxy of GaN/AlN heterostructures. Detailed chemical and thermal cleaning processes can be found in previous publications (56). Si-doped n-type GaN nanowire template was first grown at a substrate temperature of 780 °C. The growth duration of the GaN nanowire is 60 min and 20 min in Series A and B, respectively. Then, Si-doped n-type AlN nanowires of ~180 nm were grown at a substrate temperature of 910 °C. GaN/AlN digital alloys in the active region of samples were grown using identical conditions, including a substrate temperature of 910 °C and N-rich conditions with the nominal Ga/N ratio of ~0.3 and Al/N ratio of ~0.25, except for the number of periods and GaN ML and AlN thickness which can be found in Table 1. The growth rate was ~0.1 monolayer/s. During the growth of deep UV nanowire LED structure, an Mg-doped p-type AlN segment and GaN contact layer were grown on top of the active region, wherein the Ga/N ratio of 0.2 and Al/N ratio of 0.2 were used. The method for achieving effective p-type doping in AlN nanostructure can be found in our previous reports (41).

Device Fabrication. The deep UV LED fabrication starts with atomic layer deposition (ALD) of 60 nm SiO_2 to passivate the sidewall of the nanowire arrays and planarize the nanowire array. Then, a top–down etching process is performed using fluorine-based reactive ion etching (RIE) to reveal the top p-Al(Ga)N of the nanowire array. Another 200 nm SiO_2 was deposited by plasma-enhanced chemical vapor deposition (PECVD). The current injection window is designed by lithography followed by another fluorine-based RIE. The metal contact on top of the nanowire LED was fabricated based on lithography and metallization of 10 nm Ni and 10 nm Au. Finally, metal pads of 80 nm Au and backside coating of 20 nm Ti and 80 nm Au were fabricated.

Characterizations. The GaN/AlN nanowires for STEM characterizations were mechanically removed from the epitaxial Si substrates and dispersed on a lacy carbon film mesh Cu TEM grid. The JEOL JEM3100R05 TEM with double aberration correctors operated in STEM mode was utilized for HAADF imaging with a detector collection inner angle of ~79 mrad. The optical characterizations were performed using a 193 nm ArF laser. Temperature-dependent PL measurements were performed with the sample mounted on a temperature-controlled cryogenic stage. Current–voltage characteristics measurements were performed using a Keithley 2400 source meter. Electroluminescence was measured using a UV optical fiber coupled to an iHR550 spectrometer equipped with a liquid nitrogen-cooled CCD camera.

First-principles DFT Calculations. The energy change of Al-to-Ga exchange in GaN was investigated by the Vienna Ab-initio Simulation Package (VASP) with the revised Perdew–Burke–Ernzerhof (RPBE) of the generalized gradient approximation (GGA). PAW pseudopotential was used to describe the interaction between ionic and valence electrons. The 3 × 3 supercell with 5 Ga–N layers and 1 × 3 supercell with 8 Ga–N layers were used to simulate GaN(00$\bar{1}$) and GaN(1$\bar{1}\bar{3}$) surfaces, respectively. The cutoff energy of 400 eV and energy convergence of 1 × 10^{-4} eV were used in all geometry optimization calculations at the Gamma point. The energy change (ΔE) of Al-to-Ga exchange was calculated by the following formula:

$$\Delta E = E_{\text{after}} - E_{\text{before}}$$

where E_{after} and E_{before} were the free energy of the model after and before exchanging Al and Ga, respectively. A negative ΔE describes the decrease of free energy of the model after the atomic exchanges. Additionally, larger supercells (6 × 6 for polar plane and 2 × 6 for semipolar plane) have also been considered in the calculation of ΔE. A change of less than 0.15 eV was observed on ΔE, demonstrating the high accuracy of current calculations as shown in *SI Appendix*, Fig. S7.

Data, Materials, and Software Availability. All study data are included in the article and/or *SI Appendix*.

ACKNOWLEDGMENTS. This work was supported by NSF (DMR-2118809) and the W. M. Keck Foundation. Y.X. acknowledges the support from the NSF Graduate Research Fellowship under Grant 1841052. We appreciate the discussions with Ying Zhao on the first-principles DFT calculations.

Author affiliations: [a]Department of Electrical Engineering and Computer Science, University of Michigan, Ann Arbor, MI 48109; and [b]Department of Materials Science and Engineering, University of Michigan, Ann Arbor, MI 48109

Author contributions: Y.W. and Z.M. designed research; Y.W., P.Z., Y.X., K.S., D.W., and P.W. performed research; Y.W., P.Z., Y.X., K.S., D.W., P.W., and Z.M. analyzed data; and Y.W., P.Z., Y.X., and Z.M. wrote the paper.

1. U. K. Mishra, P. Parikh, W. Yi-Feng, AlGaN/GaN HEMTs–An overview of device operation and applications. *Proc. IEEE* **90**, 1022–1031 (2002).
2. J. Simon, V. Protasenko, C. Lian, H. Xing, D. Jena, Polarization-induced hole doping in wide-band-gap uniaxial semiconductor heterostructures. *Science* **327**, 60–64 (2010).
3. Y. Wu *et al.*, InGaN micro-light-emitting diodes monolithically grown on Si: Achieving ultra-stable operation through polarization and strain engineering. *Light Sci. Appl.* **11**, 294 (2022).
4. M. S. Miao *et al.*, Polarization-driven topological insulator transition in a GaN/InN/GaN quantum well. *Phys. Rev. Lett.* **109**, 186803 (2012).

5. O. Landré *et al.*, Elastic strain relaxation in GaN/AlN nanowire superlattice. *Phys. Rev. B* **81**, 153306 (2010).
6. A. Pandey *et al.*, Strain-engineered N-polar InGaN nanowires: Towards high-efficiency red LEDs on the micrometer scale. *Photonics Res.* **10**, 2809–2815 (2022).
7. Z. Zheng *et al.*, Gallium nitride-based complementary logic integrated circuits. *Nat. Electronics* **4**, 595–603 (2021).
8. Y. Li *et al.*, Dopant-free GaN/AlN/AlGaN radial nanowire heterostructures as high electron mobility transistors. *Nano Lett.* **6**, 1468–1473 (2006).
9. J. P. Reithmaier *et al.*, Strong coupling in a single quantum dot-semiconductor microcavity system. *Nature* **432**, 197–200 (2004).
10. J. Stachurski, S. Tamariz, G. Callsen, R. Butte, N. Grandjean, Single photon emission and recombination dynamics in self-assembled GaN/AlN quantum dots. *Light Sci. Appl.* **11**, 114 (2022).
11. R. Chaudhuri *et al.*, A polarization-induced 2D hole gas in undoped gallium nitride quantum wells. *Science* **365**, 1454–1457 (2019).
12. T. Oto, R. G. Banal, K. Kataoka, M. Funato, Y. Kawakami, 100 mW deep-ultraviolet emission from aluminium-nitride-based quantum wells pumped by an electron beam. *Nat. Photonics* **4**, 767–770 (2010).
13. Y. Wang *et al.*, Deep ultraviolet light source from ultrathin GaN/AlN MQW structures with output power over 2 watt. *Adv. Opt. Mater.* **7**, 1801763 (2019).
14. N. Nakagawa, H. Y. Hwang, D. A. Muller, Why some interfaces cannot be sharp. *Nat. Mater.* **5**, 204–209 (2006).
15. S. M. Islam *et al.*, MBE-grown 232–270 nm deep-UV LEDs using monolayer thin binary GaN/AlN quantum heterostructures. *Appl. Phys. Lett.* **110**, 041108 (2017).
16. H. Kobayashi, S. Ichikawa, M. Funato, Y. Kawakami, Self-limiting growth of ultrathin GaN/AlN quantum wells for highly efficient deep ultraviolet emitters. *Adv. Opt. Mater.* **7**, 1900860 (2019).
17. B. Sheng *et al.*, Individually resolved luminescence from closely stacked GaN/AlN quantum wells. *Photonics Res.* **8**, 610 (2020).
18. B. Mazumder *et al.*, Asymmetric interfacial abruptness in N-polar and Ga-polar GaN/AlN/GaN heterostructures. *Appl. Phys. Lett.* **101**, 091601 (2012).
19. I. Sayed *et al.*, Electrical properties and interface abruptness of AlSiO gate dielectric grown on 000 1 ¯ N-polar and (0001) Ga-polar GaN. *Appl. Phys. Lett.* **115**, 172104 (2019).
20. I. Lahiri, D. D. Nolte, E. S. Harmon, M. R. Melloch, J. M. Woodall, Ultrafast-lifetime quantum wells with sharp exciton spectra. *Appl. Phys. Lett.* **66**, 2519–2521 (1995).
21. D. Bayerl *et al.*, Deep ultraviolet emission from ultra-thin GaN/AlN heterostructures. *Appl. Phys. Lett.* **109**, 241102 (2016).
22. M. Nemoz *et al.*, Interdiffusion of Al and Ga in AlN/AlGaN superlattices grown by ammonia-assisted molecular beam epitaxy. *Superlattices Microstruct.* **150**, 106801 (2021).
23. V. Davydov *et al.*, The effect of interface diffusion on Raman spectra of wurtzite short-period GaN/AlN superlattices. *Nanomaterials (Basel)* **11**, 2396 (2021).
24. B. Liu *et al.*, Composition pulling effect and strain relief mechanism in AlGaN/AlN distributed Bragg reflectors. *Appl. Phys. Lett.* **98**, 261916 (2011).
25. J. Neugebauer, T. Zywietz, M. Scheffler, J. Northrup, Theory of surfaces and interfaces of group III-nitrides. *Appl. Surface Sci.* **159**, 355–359 (2000).
26. P. Bogusławski, K. Rapcewicz, J. J. Bernholc, Surface segregation and interface stability of AlN/GaN, GaN/InN, and AlN/InN 0001 epitaxial systems. *Phys. Rev. B* **61**, 10820–10826 (2000).
27. J. E. Northrup, R. Di Felice, J. Neugebauer, Atomic structure and stability of AlN(0001) and (000_1) surfaces. *Phys. Rev. B* **55**, 13878–13883 (1997).
28. N. Gao *et al.*, Integral monolayer-scale featured digital-alloyed AlN/GaN superlattices using hierarchical growth units. *Cryst. Growth Des.* **19**, 1720–1727 (2019).
29. M. Shan *et al.*, Deep UV laser at 249 nm based on GaN quantum wells. *ACS Photonics* **6**, 2387–2391 (2019).
30. B. Mazumder *et al.*, Atom probe analysis of AlN interlayers in AlGaN/AlN/GaN heterostructures. *Appl. Phys. Lett.* **102**, 111603 (2013).
31. T. Rieger *et al.*, Strain relaxation and ambipolar electrical transport in GaAs/InSb core-shell nanowires. *Nanoscale* **9**, 18392–18401 (2017).
32. O. Arif *et al.*, Growth and strain relaxation mechanisms of InAs/InP/GaAsSb core-dual-shell nanowires. *Cryst. Growth Des.* **20**, 1088–1096 (2020).
33. Y. Wu *et al.*, Monolayer GaN excitonic deep ultraviolet light emitting diodes. *Appl. Phys. Lett.* **116**, 013101 (2020).
34. A. T. Sarwar, B. J. May, M. F. Chisholm, G. J. Duscher, R. C. Myers, Ultrathin GaN quantum disk nanowire LEDs with sub-250 nm electroluminescence. *Nanoscale* **8**, 8024–8032 (2016).
35. N. Gogneau *et al.*, Influence of AlN overgrowth on structural properties of GaN quantum wells and quantum dots grown by plasma-assisted molecular beam epitaxy. *J. Appl. Phys.* **96**, 1104–1110 (2004).
36. A. R. Smith, R. M. Feenstra, D. W. Greve, J. Neugebauer, J. E. Northrup, Reconstructions of the GaN(0001¯) surface. *Phys. Rev. Lett.* **79**, 3934–3937 (1997).
37. P. Mutombo, O. Romanyuk, Ab initio density functional theory study of non-polar (101¯), (112¯) and semipolar 202¯1 GaN surfaces. *J. Appl. Phys.* **115**, 203508 (2014).
38. S. Cosentino *et al.*, The role of the interface in germanium quantum dots: When not only size matters for quantum confinement effects. *Nanoscale* **7**, 11401–11408 (2015).
39. X. Rong *et al.*, High-output-power ultraviolet light source from quasi-2D GaN quantum structure. *Adv. Mater* **28**, 7978–7983 (2016).
40. Y. Wu *et al.*, Perspectives and recent advances of two-dimensional III-nitrides: Material synthesis and emerging device applications. *Appl. Phys. Lett.* **122**, 160501 (2023).
41. Y. Wu *et al.*, Controlling defect formation of nanoscale AlN: Toward efficient current conduction of ultrawide-bandgap semiconductors. *Adv. Electron. Mater.* **6**, 2000337 (2020).
42. J. Zhao *et al.*, High internal quantum efficiency of nonpolar a-plane AlGaN-Based multiple quantum wells grown on r-plane sapphire substrate. *ACS Photonics* **5**, 1903–1906 (2018).
43. M. A. Khan *et al.*, Beyond 53% internal quantum efficiency in a AlGaN quantum well at 326 nm UVA emission and single-peak operation of UVA LED. *Opt. Lett.* **45**, 2563 (2020).
44. L. Wei-Chih, Y. Ya-Yu, H. Ray-Hua, Efficiency improvement of short-period InGaN/GaN multiple-quantum well solar cells with <formula formulatype="inline"><tex Notation="TeX">${\hbox{H}}_{2}$</tex></formula> in the GaN cap layer. *J. Display Technol.* **9**, 953–956 (2013).
45. S. Matta *et al.*, Influence of the heterostructure design on the optical properties of GaN and Al0.1Ga0.9N quantum dots for ultraviolet emission. *J. Appl. Phys.* **122**, 085706 (2017).
46. S.-H. Park, S.-L. Chuang, Spontaneous polarization effects in wurtzite GaN/AlGaN quantum wells and comparison with experiment. *Appl. Phys. Lett.* **76**, 1981–1983 (2000).
47. K. Muller-Caspary *et al.*, Electrical polarization in AlN/GaN nanodisks measured by momentum-resolved 4D scanning transmission electron microscopy. *Phys. Rev. Lett.* **122**, 106102 (2019).
48. A. M. Chowdhury *et al.*, Temperature dependent "S-Shaped" photoluminescence behavior of InGaN nanolayers: Optoelectronic implications in harsh environment. *ACS Appl. Nano Mater.* **3**, 8453–8460 (2020).
49. Q. Sun, C. D. Yerino, B. Leung, J. Han, M. E. Coltrin, Understanding and controlling heteroepitaxy with the kinetic Wulff plot: A case study with GaN. *J. Appl. Phys.* **110**, 053517 (2011).
50. V. Jindal, F. Shahedipour-Sandvik, Theoretical prediction of GaN nanostructure equilibrium and nonequilibrium shapes. *J. Appl. Phys.* **106**, 083115 (2009).
51. J. Zúñiga-Pérez *et al.*, Polarity in GaN and ZnO: Theory, measurement, growth, and devices. *Appl. Phys. Rev.* **3**, 041303 (2016).
52. K. Hestroffer, C. Leclere, C. Bougerol, H. Renevier, B. Daudin, Polarity of GaN nanowires grown by plasma-assisted molecular beam epitaxy on Si(111). *Phys. Rev. B* **84**, 172101 (2011).
53. S. M. Sadaf *et al.*, An AlGaN core–shell tunnel junction nanowire light-emitting diode operating in the ultraviolet-C band. *Nano Lett.* **17**, 1212–1218 (2017).
54. Y. Wu *et al.*, III-nitride nanostructures: Emerging applications for Micro-LEDs, ultraviolet photonics, quantum optoelectronics, and artificial photosynthesis. *Progr. Quant. Electron.* **85**, 100401 (2022).
55. V. Consonni, M. Knelangen, L. Geelhaar, A. Trampert, H. Riechert, Nucleation mechanisms of epitaxial GaN nanowires: Origin of their self-induced formation and initial radius. *Phys. Rev. B* **81**, 085310 (2010).
56. A. Aiello *et al.*, Deep ultraviolet luminescence due to extreme confinement in monolayer GaN/Al(Ga) N nanowire and planar heterostructures. *Nano Lett.* **19**, 7852–7858 (2019).